Korean Journal of Remote Sensing, Vol.27, No.3, 2011, pp.369~377

In Orbit Radiometric Calibration Tests of COMS MI Infrared Channels

Kyoung-Wook Jin† and Seok-Bae Seo

Korea Aerospace Research Institute, Daejeon, KOREA

Abstract : Since well-calibrated satellite data is critical for their applications, calibration and validation of COMS science data was one of the key activities during the IOT. COMS MI radiometric calibration process was divided into two phases according to the out-gassing of the sensor: calibrations of the visible (VI) and infrared (IR) channels. Different from the VIS calibration, the calibration steps for the IR channels followed additional processes to secure their radiometric performances. Primary calibration steps of the IR were scan mirror emissivity correction, midnight effect compensation, slope averaging and 1/f noise compensation after a nominal calibration. First, the scan mirror emissivity correction was conducted to compensate the variability of the scan mirror emissivity driven by the coating material on the scan mirror. Second, the midnight effect correction was performed to remove unreasonable high spikes of the slope values caused by the excessive radiative sources during the local midnight. After these steps, the residual (difference between the previous slope and the given slope) was filtered by a smoothing routine to eliminate the remnant random noises. The 1/f noise compensation was also carried out to filter out the lower frequency noises caused from the electronics in the Imager. With through calibration processes during the entire IOT period, the calibrated IR data showed excellent performances.

Key Words : COMS, Infrared, MI, Radiometric Calibration.

1. Introduction

COMS began to release official data to public from April, 2011(10-month after the successful launch). Two scientific payloads on COMS(MI and GOCI) will play a critical role for various researches of land, ocean and atmosphere focused on the Korean peninsular. After the COMS Launch, IOT(In-Orbit Test) was conducted intensively. The IOT is crucial since the BUS and all subsystems of the COMS, which passed the ground test, are tested again and verified in a harsh space environment in this period.

Various functional and performance tests were carried out during the about seven month IOT period thoroughly. Main activities were rigorous tests for the payloads. Table 1 shows a summary of the IOT activities according to the IOT phases.

Radiometric calibration processes were mainly performed during the Phase 1 and Phase 5. Because of the out-gassing, which is a process to eliminate

Received April 30, 2011; Revised June 17, 2011, Revised June 22, 2011; Accepted June 23, 2011.

† Corresponding Author: Kyoung-Wook Jin (kwjin@kari.re.kr)

Table 1. Major test items during the IOT according to its pahses.

IOT Phases	TESTS	PERIOD
BUS IOT	Functional tests of BUS and satellite sub-systems	Launch ~ Early of July, 2010
Switch-Over	Switch over of COMS operation after LEOP& MODCS test	2 weeks after the Launch
Phase 1	MODCS test & Radiometric functional and performance tests of MI and GOCI	July, 2010 ~ Jan, 2011
Phase 2	INR Functional tests of MI and GOCI	July, 2010 ~ Jan, 2011
Phase 3	Ka-band antenna beam test(South Korea-beam and North Korea-beam antenna pattern test)	July, 2010
Phase 4	Antenna deploy and trimming mechanism(ADTM) adjustment and Ka-band China beam test	Aug, 2010
Phase 5	MI Visible and Infrared channel functional and performance tests for radiometric calibrations	Aug, 2010~ Jan, 2011
Phase 6	MI(VIS +IR) and GOCI INR functional and performance test	Aug, 2010~ Jan, 2011

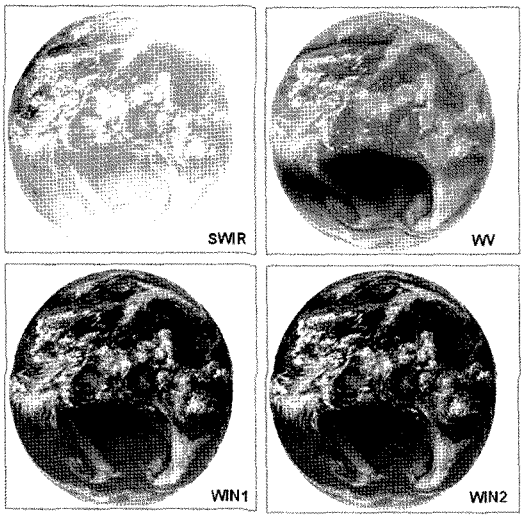

Fig. 1. First COMS IR Raw(Level 0) images(2010.8.11, 10:12 UTC). SWIR, WV, WIN1, and WIN2 represents shortwave, water vapour, window 1 and window 2 channels respectively.

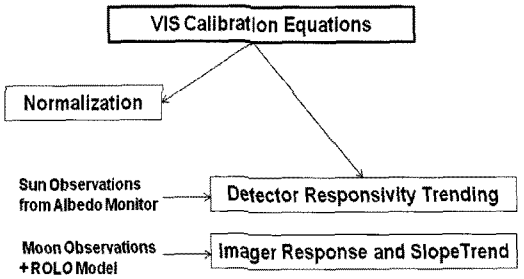

Fig. 2. COMS MI Visible Channel Calibration Process.

remnant volatile materials, radiometric calibration activity was partitioned into two periods: before and after the out-gassing. Improper out-gassing can lead to harmful impacts(e.g. degradation of the image quality) on an optical payload on a spacecraft. The COMS out-gassing was performed carefully by heating MI(Meteorological Imager) sensors about 42 days after the satellite launch. During this time, the cooling cover was closed to prohibit the passive cooling process which is necessary for operating IR sensors. Thus, the IR channels of MI were off(not operating) during the out-gassing. After the successful out-gassing tests, the IR channels were switched on and the first raw images taken from the IR channels showed reasonable performance even without the calibrations(Fig. 1).

The accurate calibration is directly related with the accurate image qualities. Geometric calibration(or INR), the post-calibration just after the radiometric calibration, is also affected by the radiometric calibration status of the data. For example, the threshold value for a cloud detection algorithm embedded in the INR is set up based on the qualified radiometric performance of the data.

In addition, the qualities of various Level 2 products(Chung *et al.*, 2006; Ha *et al.*, 2006; Yoo *et al.*, 2006; Hong *et al.*, 2009), which are retrieved based on the COMS MI data highly depend on the data calibrations.

Compared to the visible channel' s calibration, that of the IR was more complex. Fig 2 and Fig 3 show the difference between the two processes: VIS and IR calibrations respectively. Required additional sequences for the IR data processing includes a scan

Table 2. COMS MI channels and their corresponding wavelengths.

Channels	Wavelength(μm)
VIS	0.675 (0.55-0.80)
SWIR	3.75 (3.50-4.0)
WV	6.75 (6.5-7.0)
WIN1	10.8 (10.3-11.3)
WIN2	12.0 (11.5-12.5)

mirror emissivity correction, a midnight effect correction, slope averaging, and the 1/f noise compensation.

2. Method

Table 2 indicates center wavelengths and their spectral responsivity ranges of the VIS and four IR channels of the MI instrument. The MI's four IR bands(Fig. 4) are very similar with its spectral ranges with respect to the previous heritage Imagers(GOES-8 & GOES-12). Its performance is, however, more improved(comparable with MTSAT-2 imager and GOES-13 imager).

Nominal(basic) calibration equations for VIS and IR are expressed as

$$R = m \times X + b, \tag{1}$$

$$R = q \times X^2 + m \times X + b, \tag{2}$$

where R is radiance(W/m^2 · sr · μm), X is digital counts, q is a priori(determined before launch), m is gain(or slope) and b is offset(intercept) respectively. The slope(m) is determined by

$$m = \frac{R_{BB} - q(X^2_{BB} - X^2_{BB})}{X_{BB} - X_{SP}} \tag{3}$$

where $_{BB}$ is the black body observation and $_{SP}$ is the space look.

The IR calibration equation(Eq.(2)) use a 2nd order polynomial fitting compared to a simple linear fit of the VIS(Eq.(1)) to account for some of non-linearity

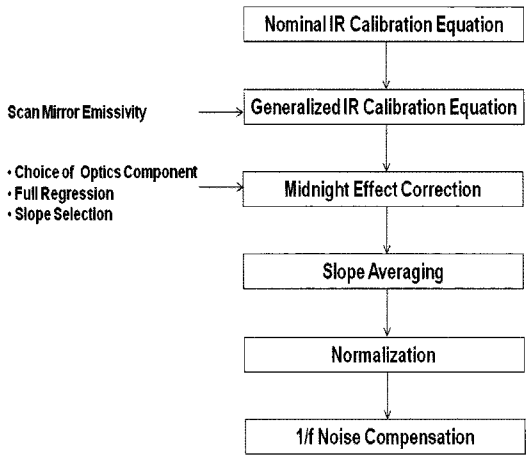

Fig. 3. COMS MI Infrared Channel Calibration Process.

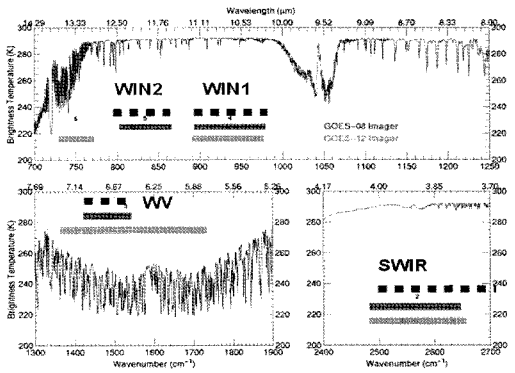

Fig. 4. Wavelengths of MI five channels(WIN2, WIN1, WV and SWIR) compared with corresponding GOES imager channels. Dotted line denotes COMS channels.

between the digital counts and the radiance of the IR data. The key parameter of the slope value, m on the basic equation (1 & 2), is determined based on the two lower and upper limits of observations(cold end of the space look and warm end of the black body counts) as expressed in Eq.(3). After the validation of the nominal calibration equations(from the comparison between the computed value and the results from the COMS IMPS(Image pre-processing system)), intensive processing for removing additional error sources was conducted step-by-step(see Fig. 3)

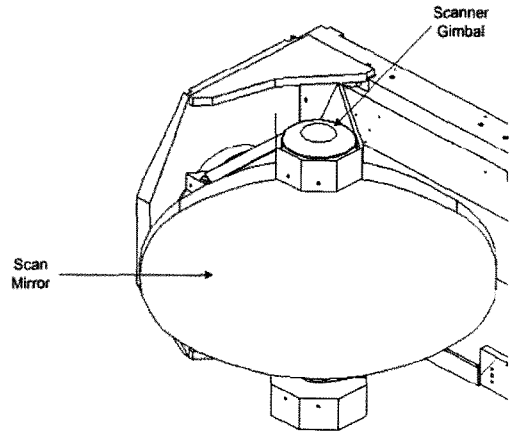

Fig. 5. Schematic of the MI scan mirror.

1) Scan Mirror Emissivity Correction(SMEC)

An ideal imager should be independent on a change of the scan angle, especially during a space look measurement. In practice, the different scan mirror angle and scan mirror temperature significantly affects the radiometry of the instrument. This scan mirror emissivity effect is attributed to a coating material on the scan mirror(Fig. 5). The emissivity is varied with the different angles of the scan mirror during the scanning. To remove this error, the diurnal variation of the scan mirror emissivity during a 24hr period is modelled as follows.

$$\varepsilon(\theta) = a_0 + a_1 \times \theta + a_2 \times \theta^2 \qquad (4)$$

Eq.(4) represents the emissivity variation as a function of a E-W scan angle, θ. The dark images, which take dark space observations(cold cosmic background), measure the emissivity variation according to different scan angles. More detailed description for the scan mirror emissivity correction(SMEC) can be found from(Chang *et al.* 2007; Seo *et al.* 2011).

2) Midnight Blackbody Calibration Correction (MBCC)

During a local midnight, there are additional energy sources(e.g. stray light) which give an impact to the radiometry of the instrument. While a black body absorbs the radiation 100 % and re-emit the radiation ideally, some parts of the energy are reflected from the black body target inside the Imager actually. This excessive energy coming into the detectors of IR channels, which is robust during a midnight, can lead to additional errors.

To eliminate the Midnight effect, an algorithm (Ledez, 2010) was carefully designed based on previous studies(Weinreb, 1996). For a nominal IR calibration mainly conducted based on the black body(BB) calibration target measurement and cold space look, the BB is performed every 30 minutes. The Midnight effect can be readily observed from a sharp increase of the slopes of BB near midnight. Basic idea is to utilize the correlated optics temperature rather than the actual slope values. From the regression-based estimated slopes, erroneous slopes which contain the mid night' s extra radiances are removed.

3) Slope Averaging

Dominant errors(systematic and random errors) of IR channels are removed mainly from the key radiometric calibrations steps(Nominal IR calibration equation with the SMEC and the MBCC). However, the responsivity change of the detectors driven by unknown diurnal variations due to the background radiation change inside the Imager can be eliminated by a smoothing process(average over slopes) as well. This random error on the responsivity occurs independently for two detectors of each frequency. For the slope averaging process, it is simply assumed that the behaviour of the slope's variation is stable up

to two or three days. The difference between the slopes of the previous day and current day are filtered by the smoothing.

4) 1/f Noise Compensation

A 1/f noise(or pink noise) is a type of electronic noise. Usually it occurs on almost all electronic devices. The power spectral density(representation of the noise) is inversely proportional to the frequency. The 1/f noise, which is dominant in a lower frequency regime, is interpreted as a random bias of the output signals from the IR detectors. Since the 1/f noise has a larger impact especially on the water vapour(WV) channel(~6.75μm), the effective implementation of the 1/f noise compensation can remove the stripping effect on the WV channel significantly. The lower frequency component noises are filtered out using the assumption that the variation of radiance per each line is less than the random noise from the detectors.

3. Results

The scan mirror emissivity variation was estimated using the dark image data. In Fig 6, scan mirror emissivity varies according to different scan elements (or scan angles). The scanning was conducted from the West space look side(45°-10.4°/2) to the East space look side(45°+10.4°/2). The middle of the scan element coreresponds to 45°scan angle(nadir position). Single observaton consists of total 10 scan lines and entire dark imaing(~54mintutes) comprises the 30 observations(300 lines). The fitted line overlapped with the original data denotes the scan mirror emissivity with a scan angle. The approximated coffecient values are listed in the Table 3.

To account for the 24hr variation of the emissivity (diurnal effect), special 24hr dark image data were

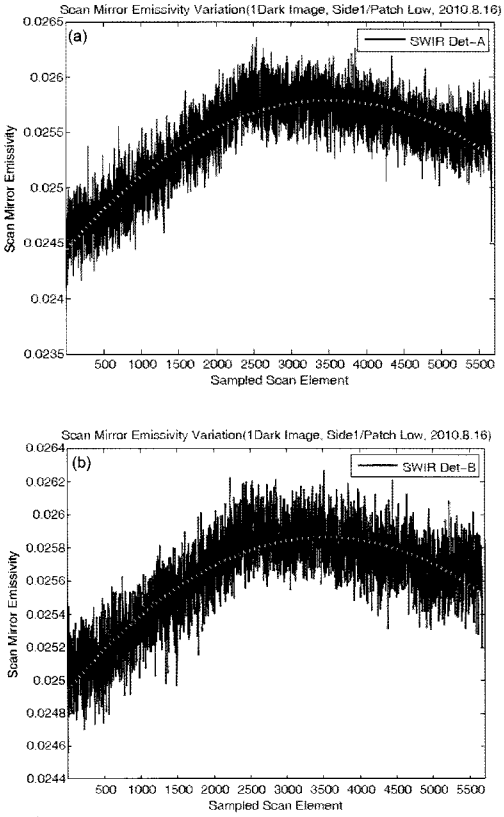

Fig. 6. Scan mirror emissivity as a function of a scan angle for(a) SWIR det-A and(b) det-B(2010.8.16, Side1/Patch Low case). 1hr dark images were used for the analyses. Dotted lines represents a linear fit.

Table 3. Computed scan mirror emissivity coeffients from the 1hr dark image data.(side1/patch low, 2010.12.10)

Channel	Detector	Coef_a0	Coef_a1	Coef_a2
SWIR	A	2.59E-02	1.00E-07	7.18E-13
SWIR	B	2.57E-02	8.46E-08	-1.81E-13
WV	A	1.89E-02	2.40E-07	1.83E-11
WV	B	1.90E-02	1.99E-07	2.52E-11
WIN1	A	2.08E-02	8.55E-07	-3.65E-11
WIN1	B	2.09E-02	8.45E-07	-3.55E-11
WIN2	A	2.65E-02	1.20E-06	-2.62E-11
WIN2	B	2.63E-02	1.21E-06	-1.42E-11

taken and analyzed during the IOT. Table 4 shows the coeffients from 24 hrs data. Since SWIR (~3.75μm) chanel is close to VIS electromagnetic range, where the reflective energy is more dominant,

Table 4. Computed scan mirror emissivity coeffients from the 24hr dark image data(side1/patch low, 2010.8.17, 14:12UTC ~ 2010.8.18, 14:12 UTC)

Channel	Detector	Coef_a0	Coef_a1	Coef_a2
SWIR	A	2.594E-02	0.0	0.0
SWIR	B	2.574E-02	0.0	0.0
WV	A	1.858E-02	5.962E-08	9.516E-13
WV	B	1.858E-02	5.962E-08	9.516E-13
WIN1	A	1.971E-02	2.487E-07	-2.426E-12
WIN1	B	1.946E-02	2.821E-07	-3.555E-12
WIN2	A	2.534E-02	2.892E-07	-6.008E-13
WIN2	B	2.505E-02	3.132E-07	-1.027E-12

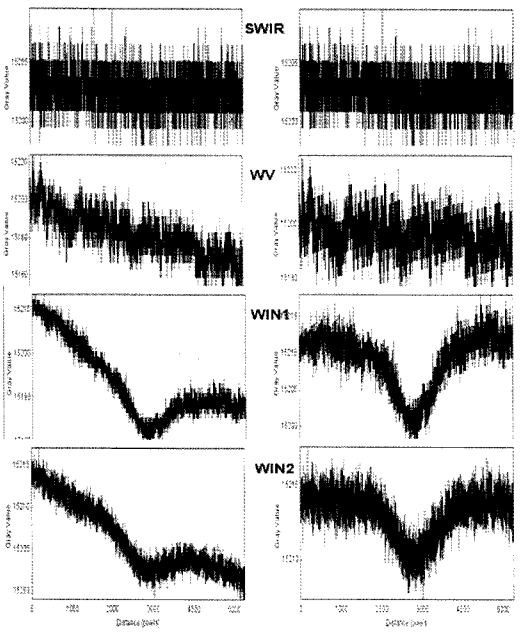

Fig. 7. The results of the before(left) and after(right) scan mirror emissivity compensation.10 first northern lines profiles of IMPS LV1A images were used(courtesy of Ledez).

the emissivity variation compared to other channels is very minimal. It is also noted that the coating material of SiO2 was replaced with MgF2 to reduce the effects of the scan mirror emissivity on the COMS IR channel radiometry.

Based on the estimated equations(scan mirror emissivity compensation algorithm based on Table 4), the scan mirror emissivity effect was removed properly in the IMPS.

As observed from Fig. 7, the scan mirror effect compensated data(right-hand side) shows reasonable behaviour. For this test, the 10 northern lines of space look observations in the Level1A data were used. The concave shape in the middle of figures represents the stray light effect coming from the Earth(the measurement was conducted near the Earth Limb). It is noted that higher digital counts(Y axis) are corresponding to colder temperature at the IR channels. The mean space look on the both sides(East and West) is consistent each other as a results of the scan mirror emissivity compensation.

To monitor the behaviour of the scan mirror emissivity within the mission life time of COMS(~7yrs) continuously, regular 1dark image observations on every three month are required.

The effect of the Midnight effect is clearly shown in Fig. 8: near slope ID 15(close to a midnight, 15UTC in Fig 8c). It is straight forward that this unreasonable higher slope value can lead to calibration errors. The Midnight effect correction was performed after the scan mirror effect adjustment(see Fig 3). The process of the Midnight effect correction was divided into three steps: 1) Choice of optics, 2) Full regression, and 3) Slope selection.

Fig. 8 shows the sequence of the Midnight effect correction process. First, out of several optics of the sensor(e.g. Scan mirror, Primary telescope, Secondary telescopes, Primary baffle, etc), a correlated optic temperature with the BB slope was chosen. Fig 8a shows comparison between the slope of BB and the scan mirror temperature. The abrupt two spikes over slope ID 10~ 20 range indicates the Midnight effect. Except the scale difference, the behaviour of the scan mirror temperature is well correlated with the BB slope. In this case, the detector A was a set up in IMPS as a reference detector. Second, Fig 8b shows the estimated slope resulted from the full regression. The estimated slope contains the reasonable slope

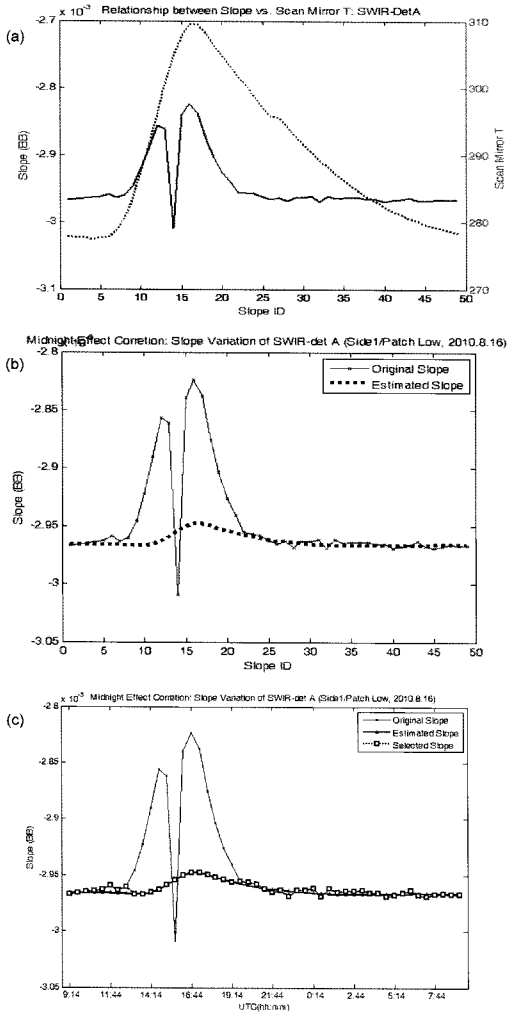

Fig. 8. The Midnight effect correction processes: (a) Choice of Optics components, (b) Full regression, and (c) Slope selection(Side1/Patch Low, 2010.8.16).

values because the contaminated data from the Midnight effect were removed.

For the MBCC, 10 consecutive days of data were prepared and processed to find optimal parameters for the effective Midnight effect correction. It was found that the reasonable number of day for the Midnight correction was five days since the fitting accuracy was decreasing(fitting error is increasing) significantly after five days. This result represents that the slope variation is stable within the 5 days and thus the applied Midnight effect correction is valid within

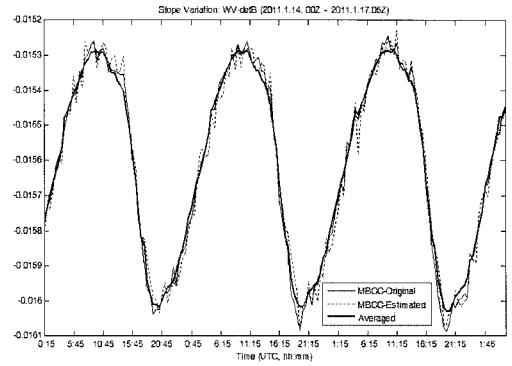

Fig. 9. Result of the slope averaging with the Midnight effect compensation.

5 days. However, this statement is only valid during the non-eclipse period(eclipse data were not analyzed for MBCC during the IOT). From this MBCC compensation, the slope values around +- 4 hours from the midnight are replaced with that of the estimated slope.

Finally Fig 8c shows the selected slope compared to the original slope. As expected, the selected slopes comprise the estimated slopes around midnight and the black body slopes during the rest of times.

Fig. 9 shows the diffrence between the averaged slope(thick line) and the original slope(thin line). The noise pattern observed from the MBCC-estimated (without the slope averaging) were considerabley reduced in the averaged slope.

Primary 1/f algorithm parameters in the IMPS(Ledez, 2008) are comprised of four items: fs(EW Sampling Frequency), N(Number of lines for the comparison), CoeffC(for weighting) and fc(Cut-off Frequency).The values of the fs and N was set up as a constant(fs=218400/4 Hz and N=3 respectively) and the finally adjusted parameters based on the IOT data from IMPS are shown in Table 5.

As a performance evaluation of the calibrated IR data, consecutive slope of 13 days(Oct 27, 2010 ~ Nov 9, 2010) was examined. The 13 peaks observed in the MBCC-original slope(see Fig. 10) clearly

Table 5. 1/f Noise compensation parameters(SIDE1, Patch Low)

Channels	CoeffC ($W \cdot m^{-2} \cdot sr^{-1} \cdot \mu^{-1}$)	f_c(Hz)
SWIR	*no 1/f noise filtering required*	*no 1/f noise filtering required*
WV	4.6 x 10-2	120
WIN1	1.8 x 10-2	50
WIN2	2.4 x 10-2	30

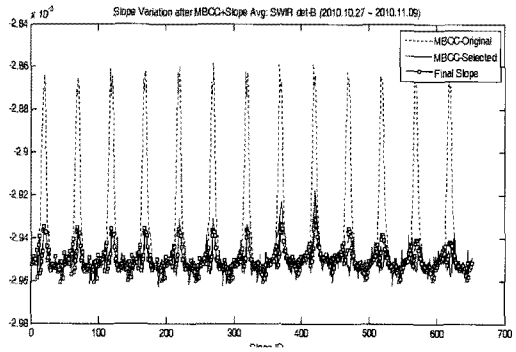

Fig. 10. Final slope with all required IR calibration processes (SMEC, MBCC, Slope averaging and 1/f noise compensation)

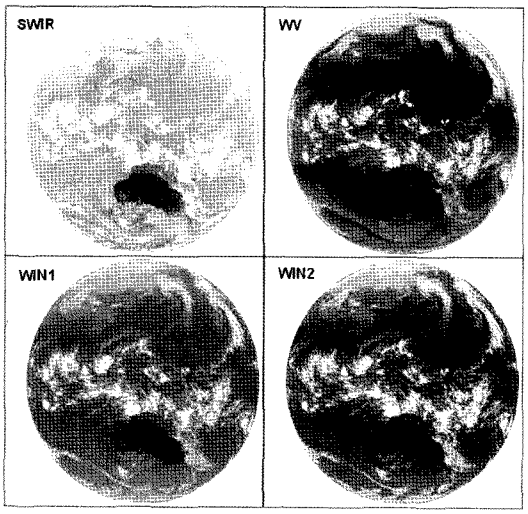

Fig. 11. Calibrated Level 1A COMS MI IR images(2010.12.23, 02:45 UTC).

shows the impact of the Midnight effect. On the other hand, the final slope variation behaviour shows reasonable performances after the required all the IR calibration processes(SMEC, MBCC, Slope Averaging and 1/f noise compensation). The well-calibrated IR image sample is also shown in Fig. 11.

4. Conclusion

The radiometric calibration activities for the COMS MI instrument were conducted intensively during the seven-month IOT period. The calibration processes of IR channel after that of VIS channel placed a challenge due to its complexity and a stop-less real-time processing requirement of the COMS IMPS. The major calibration steps of the IR channels: SMEC, MBCC, Slop Averaging and 1/f Noise compensation, were carried out based on off-line version of the COMS IMPS. The evaluation of the calibrated MI IR data from the IMPS's operation configuration(Side 1/ Patch Low) showed excellent performances that meet all required image qualities for the radiometric accuracy of the MI.

Acknowledgements

The authors gratefully thank collaboration and many supports from C. Ledez and J.L. Duquesne (EADS Astrium) and Y.R. Lee and D.S. Kim(Satrec Initiative) during the IOT.

This work represents some parts of the researches carried out at Korea Aerospace Research Institute, under the COMS project sponsored by Ministry of Education, Science and Technology.

References

Chang, K-H., T-H. Oh, M-H. Ahn, N-S. Cho, and S-N. Oh, 2007. Investigation of NESDIS's Calibration Algorithm of the Imagers for IR

Channels on GOES-12. *Korean Journal of Remote Sensing*, 23(1): 55-58.

Chung, C-Y., H. K. Lee, H-J. Ahn, M. H. Ahn, and S. N. Oh, 2006. Developing the Cloud Detection Algorithm for COMS Meteorological Data Processing System. *Korean Journal of Remote Sensing*, 22(5): 367-372.

Ha, J-S., J-H. Kim, and H-J. Lee, 2006. The Detection of Yellow Sand with Satellite Infrared bands. *Korean Journal of Remote Sensing*, 22(5): 403-406.

Hong, K-O., M-S. Suh, and J-H. Kang, 2009. Improvement of COMS Land Surface Temperature Retrieval Algorithm. *Korean Journal of Remote Sensing*, 25(6): 507-515.

Ledez, C., 2008. COMS MI 1/f Noise Compensation Algorithm, Astrium EADS.

Ledez, C., 2010. MI Radiometric Model, Astrium EADS.

Seo, S-B., K-W. Jin, and S-I. Ahn, 2011. Scan mirror Emissivity Compensation for the COMS MI, *Aerospace Engineering and Technology*, 10(1), Korea Aerospace Research Institute, Daejeon, Korea(Accepted).

Weinreb, M.P., 1996. Real-world calibration of GOES-8 and -9 sensors, *Proc. SPIE*, 2812: 572-586.

Yoo, J-M., M-J. Jeong, H-L. Yoo, J-E. Rhee, Y-M. Hur, and M-H. Ahn, 2006. Fog Sensing over the Korean Peninsular Derived from Satellite Observation of MODIS and GOES-9. *Korean Journal of Remote Sensing*, 22(5): 373-377.